Molecular Nutrition & Food Research
www.mnf-journal.com

The Effects of Resveratrol, Caffeine, β-Carotene, and Epigallocatechin Gallate (EGCG) on Amyloid-β_{25-35} Aggregation in Synthetic Brain Membranes

*Isabella P. Gastaldo, Sebastian Himbert, Udbhav Ram, and Maikel C. Rheinstädter**

Scope: Alzheimer's disease is a neurodegenerative condition marked by the formation and aggregation of amyloid-β (Aβ) peptides. There exists, to this day, no cure or effective prevention for the disease; however, there is evidence that a healthy diet and certain food products can slow down first occurrence and progression. To investigate if food ingredients can interact with peptide aggregates, synthetic membranes that contained aggregates consisting of cross-β sheets of the membrane active fragment $A\beta_{25-35}$ are prepared.
Methods and results: The impact of resveratrol, found in grapes, caffeine, the main active ingredient in coffee, β-carotene, found in orange fruits and vegetables, and epigallocatechin gallate (EGCG), a component of green tea, on the size and volume fraction of Aβ aggregates is studied using optical and fluorescence microscopy, X-ray diffraction, UV–vis spectroscopy, and molecular dynamics simulations. All compounds are membrane active and spontaneously partitioned in the synthetic brain membranes. While resveratrol and caffeine lead to membrane thickening and reduced membrane fluidity, β-carotene and EGCG preserve or increase fluidity.
Conclusion: Resveratrol and caffeine do not reduce the volume fraction of peptide aggregates while β-carotene significantly reduces plaque size. Interestingly, EGCG dissolves peptide aggregates and significantly decreases the corresponding cross-β and β-sheet signals.

1. Introduction

A common societal concern that has been rising over the past couple of years is the prevalence of Alzheimer's disease (AD), the most common cause of dementia worldwide. In 2001, an estimated 24 million people around the world were living with dementia, a number that is expected to double every 20 years, reaching 81.1 million by 2040.[1] AD is marked clinically by gradual cognitive decline, and pathologically by the presence of senile plaques, which are formed through the aggregation of amyloid-β (Aβ) peptides in functional tissue of the brain.[2] Although the etiology of AD is not yet fully understood, there is strong evidence that aggregated Aβ peptides play a critical role in its pathogenesis.[3,4] Given the connection between Aβ and AD, one of the key theories to explain AD pathogenesis is the amyloid cascade hypothesis, which proposes that the deposition of Aβ peptides is the causative agent of AD's pathology.[5] Although the amyloid hypothesis, which identified the accumulation and deposition of oligomeric or fibrillar Aβ peptides as the primary cause of Alzheimer's disease (AD), had been disputed in recent years,[6,7] amyloid accumulation is now believed to play a crucial role in beginning the pathological process while other downstream events, such as neuroinflammation and tau accumulation are likely the main drivers of neurodegeneration.[4,8] This makes amyloid plaques a prime target for pharmaceutical development. Already today, existing pharmaceutical approaches are mostly focused on the design and synthesis of therapeutics to inhibit pathological oligomerization of amyloid and tau proteins by computer-aided drug design and medicinal chemistry.

Aβ peptides are derived by improper proteolytic cleavage of the amyloid-β precursor protein (APP), which is an integral membrane protein.[9,10] Improper cleavage increases the production of less soluble and more toxic Aβ.[11,12] The main Aβ types formed from this cleavage are $A\beta_{1-40}$ and $A\beta_{1-42}$, both of which contain the short, primarily hydrophobic amino acid fragment (25–35) which is known to embed itself into the hydrophobic core of the membrane.[13–16] As such, it is often used in membrane studies.

One of the major forms of Aβ aggregates in amyloid plaques is amyloid fibrils, composed of a cross-β spine.[17–19] These fibrils aggregate via a nucleation-dependent pathway composed of a nucleation and an elongation stage. During the nucleation stage, there is a lag phase where the nucleus accumulates and

I. P. Gastaldo, S. Himbert, U. Ram, Dr. M. C. Rheinstädter
Department of Physics and Astronomy
McMaster University
Hamilton, Ontario, L8S 4M1, Canada
E-mail: rheinstadter@mcmaster.ca
I. P. Gastaldo, S. Himbert, U. Ram, Dr. M. C. Rheinstädter
Origins Institute
McMaster University
Hamilton Ontario, L8S 4M1, Canada
I. P. Gastaldo
Department of Biochemistry and Biomedical Sciences
McMaster University
Hamilton Ontario, L8S 4M1, Canada

DOI: 10.1002/mnfr.202000632

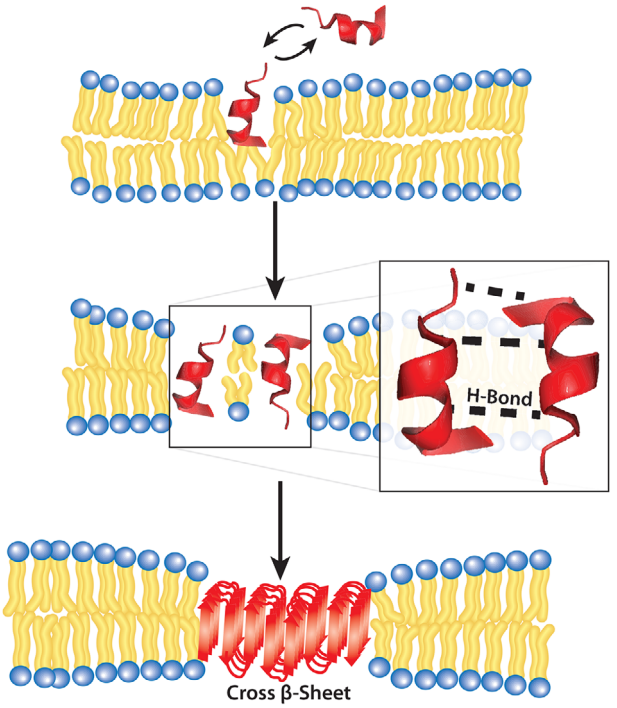

Figure 1. Aggregation pathway for Aβ_{25-35} in membranes. Aβ_{25-35} coexists in an external and inserted phase in which there is a certain free energy barrier which inhibits full insertion. For this reason, there is a rate of insertion and expulsion within the membrane. After the insertion, H-bonding between neighboring Glu and Arg residues coordinate lateral attraction and promote the formation of a cross-β sheet through the U-turn N-terminus residues external to the bilayer.

Aβ molecules are mostly amorphous monomers. During the elongation stage, these monomers assemble into oligomers, protofibrils, and mature fibrils.[20] There is strong evidence that membranes play a crucial role in the aggregation of these peptides by serving as a nucleation point,[21,22] in particular at early stages of plaque formation. The formation of amyloid fibrils and plaques starts in small, nanometer-sized peptide clusters that form within membranes in the brain and membrane properties play a decisive role if peptides aggregate.[22] As depicted in **Figure 1**, the bilayer offers a site of high stability for Aβ_{25-35} monomers with an equilibrium between adsorbed and dissolved peptides. From this, the stabilization of this inserted form allows neighboring peptides to coordinate hydrogen-bonding, and long-range lipid attractions to minimize membrane surface tension between Aβ fragments. This allows for folding and uncoiling of the peptide to form more stable cross-β sheets which makes the membrane a key mediator in the nucleation of these aggregates.

The biophysical properties of membranes influence membrane functions, as well as the activity of essential proteins that regulate our cells. It is now commonly accepted that membrane structure and dynamics are an essential contributor to membrane functionality.[23,24] Subtle modifications to the structure of membranes are therefore of vital importance in maintaining homeostasis. For instance, many neurodegenerative diseases are associated with lipid alterations.[25,26] However, the majority of drugs targeting them are designed to interact with membrane receptors or enzymes. This limitation likely reduces the efficacy of our current therapies on the progression of these diseases. Thus, making the cell membrane a target has the potential for new treatments for numerous pathologies, including AD.

Despite tremendous efforts, no progress has been made toward treating protein misfolding diseases, such as AD. However, a diverse range of bioactive nutrients found in natural products have been shown to play a potential role in the prevention of several neurodegenerative diseases.[27] Many researchers investigated the role of resveratrol,[28–32] caffeine,[33–37] β-carotene,[38–41] and epigallocatechin gallate (EGCG)[28,42–45] as potential candidates for AD intervention. Many of these molecules also resulted in changes related to memory and other cognitive functions. Resveratrol was shown to improve memory performance and facilitate memory formation in mice,[46,47] and β-carotene supplementation improved cognitive impairment and oxidative stress.[48,49] Both EGCG and caffeine were also reported to reduce cognitive impairment and prevent memory decline.[50,51]

Resveratrol is most commonly found in the skin of grapes, and is often consumed in the form of red wine. Karuppagounder et al.[29] found that resveratrol reduced amyloid induced pathology in transgenic mice and Marambaud[30] demonstrated that it promotes intracellular degradation of Aβ peptides. Feng et al.,[31] however, discovered that resveratrol inhibited or disaggregated Aβ fibrils, but could not inhibit the formation of oligomers. Lastly, Wang et al.[28] reported that resveratrol binds to Aβ peptides and converts it into disordered oligomers. Caffeine is the principal pharmacologically active component found in coffee. Maia and De Mendonça[33] reported that caffeine exposure is inversely associated with AD, a finding that was supported by Arendash et al.,[34,35] who reported that caffeine resulted in a decrease of Aβ production in transgenic mice. Simulations have also been performed to examine interactions between Aβ and caffeine. Sharma and Paul[36] found from molecular dynamics simulations that caffeine molecules can bind to Aβ and physically block amyloid formation and subsequent aggregation.

β-carotene is a naturally occurring carotenoid found in carrots as well as in other orange fruits and vegetables. Wei et al.[38] reported that people with severe AD, compared to mild AD or control, showed decreased plasma levels of β-carotene, thus suggesting that it may be used to slow the rate of cognitive decline. Similarly, Li et al.[41] have shown that β-carotene significantly improved cognitive function in the elderly. In addition, Junichi et al.[40] reported that β-carotene inhibited the oligomerization of Aβ, therefore proposing a direct interaction between β-carotene and Aβ. EGCG is abundantly found in green and white tea, with smaller amounts also found in black tea and it is known for its potent antioxidant properties. Rezai-Zadeh et al.[45] studied EGCG interactions with Aβ_{25-35} and found that it reduces Aβ generation in neuron-like cells and that EGCG resulted in a decrease of Aβ levels and plaques in transgenic mice. Bieschke et al.,[43] on the other hand, demonstrated that EGCG can bind to Aβ aggregates and convert them into smaller, amorphous protein aggregates which are non-toxic to mammalian cells. Similar results were obtained by Ehrnhoefer et al.[42] showing that EGCG directly binds to the peptide and inhibits fibrillogenesis. Interestingly, Zhang et al.[52] utilized atomistic simulations of Aβ interacting with EGCG to show that in its presence, Aβ peptides were found

to have a decrease in β-sheet content and an increase in coil and α-helix conformation.

The goal of this study is to determine if these naturally occurring molecules can change the size and volume fraction of Aβ clusters. While some of the natural compounds were reported to interact with Aβ directly, our hypothesis is that these molecules can potentially affect peptide aggregation through an indirect, membrane-mediated pathway. We, therefore, first checked if these molecules are membrane active and spontaneously partition in a synthetic brain membrane. We found that the different compounds have very different effects on Aβ aggregates: the addition of certain molecules resulted in clusters which were found to be expelled from the membrane and formed cross-β sheets or amyloid fibrils outside the membranes, whereas other molecules were found to be able to break up the cross-β sheets into smaller β-sheets or even dissolve cross-β sheets and β-sheets.

2. Experimental Section

2.1. Brain Membrane Mimics Preparation

All molecules used in this study are depicted in **Figure 2**. Synthetic anionic brain membranes were prepared from unsaturated 1-palmitoyl-2-oleoyl-sn-glycero-3-phosphocholine (POPC) and saturated, anionic 1,2-dimyristoyl-sn-glycero-3-phospho-L-serine (DMPS). The peptide segment Aβ_{25-35} was added at a peptide concentration of 20 mol% (peptide-to-lipid ratio), which spontaneously lead to the formation of nano to micrometer-sized cross-β amyloid plaques.[53,54] Solid supported membranes were prepared for the microscopy and X-ray experiments and liposomes were used in the UV–vis spectroscopy experiments.

2.2. Liposome Preparation

Solutions of POPC and DMPS at a concentration of 20 mg of lipid per mL of solvent were each dissolved in ultrapure (18.2 MΩ cm) water and sonicated for 30 min. The amyloid-β peptides were prepared by pre-treatment with trifluoroacetic acid (TFA) to disaggregate the peptide, as described in [55]. This pre-treatment included dissolving the peptide in a 1 mg mL^{-1} solution of TFA, sonicating with a tip sonicator for four 3 s intervals, and then removing the solvent through evaporation using dry nitrogen gas. The peptides were then re-dissolved in ultrapure water at a concentration of 20 mg mL^{-1}.[53,54,56,57] Stock solutions of resveratrol, caffeine, β-carotene, and EGCG were prepared at concentrations of 20 mg mL^{-1} and each solution was sonicated and vortexed until homogeneous. Liposomes of POPC and DMPS (97:3 mol per mol%) were prepared with 20 mol% of Aβ_{25-35} and incubated for 2 h. After incubation, 5 mol% of resveratrol, caffeine, β-carotene, or EGCG were added to each sample, vortexed until homogenous and incubated overnight. It was important to note that when lipids were dissolved in water, they spontaneously formed large multilamellar vesicles (MLVs). By sonication of the lipid solution, small, unilamellar vesicles (SUVs) were produced. When each molecule was then added, they interacted and embedded into these SUVs. These solutions were then directly used for the UV–vis spectroscopy measurements.

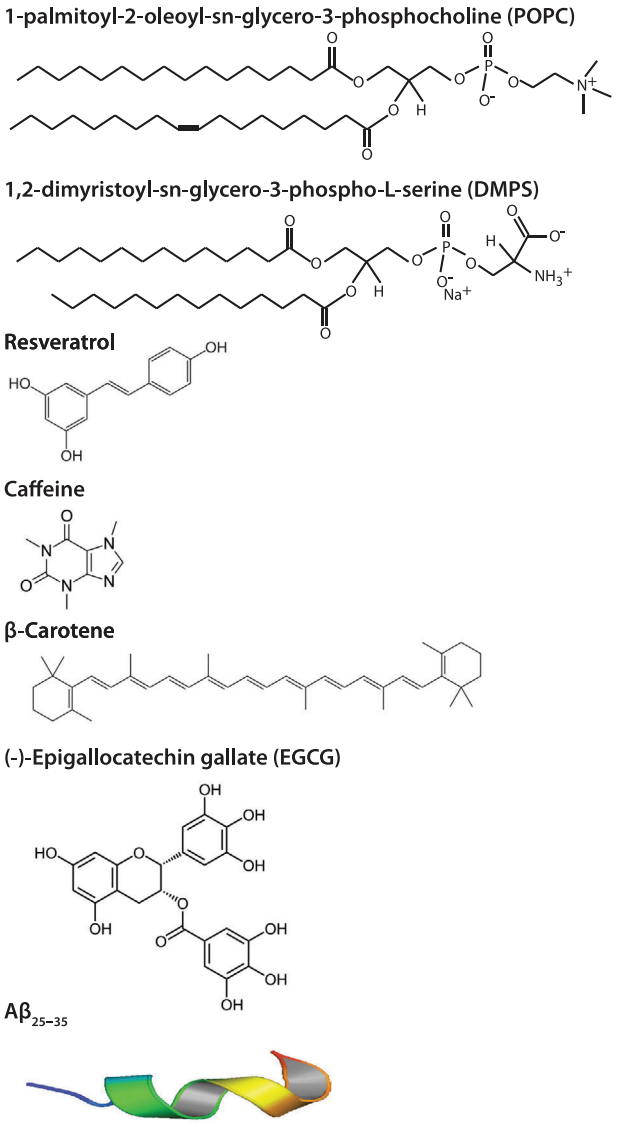

Figure 2. Schematic representation of all compounds used in this study: 1-palmitoyl-2-oleoyl-sn-glycero-3-phosphocholine (POPC), 1,2-dimyristoyl-sn-glycero-3-phosphoserine (DMPS), resveratrol ($C_{14}H_{12}O_3$), caffeine ($C_8H_{10}N_4O_2$), β-carotene ($C_{40}H_{56}$), EGCG ($C_{22}H_{18}O_{11}$), and amyloid-β_{25-35} ($C_{45}H_{81}N_{13}O_{14}S$).

2.3. Supported Membrane Preparation

In order to produce solid supported membranes, the prepared liposomes were applied on solid support for the microscopy and X-ray experiments. They were placed on single-side polished silicon wafers. 100 mm diameter, 300 µm thick silicon wafers were pre-cut into 1 × 1 cm^2 chips. The wafers were first pretreated by sonication in dichloromethane at 35 °C for 30 min to remove all organic contamination and leave the substrates in a hydrophobic state. Each wafer was thoroughly rinsed three times by alternating with ≈50 mL of distilled water and methanol.

The heating block was heated to 40°C, 65 µL of lipid solution was applied on each wafer, and the water was allowed to slowly evaporate for ≈10 min. After drying, the bilayers were incubated and rehydrated in a saturated K_2SO_4 solution overnight at 30 °C, which provided 97% relative humidity (RH). This procedure resulted in highly oriented membrane stacks that uniformly covered the silicon substrates.[53,54,56,57]

2.4. Molecular Dynamics Simulations

Molecular dynamics (MD) simulations were performed to study the interaction between the natural compounds and synthetic brain membranes. All simulations were run in-house on MacSim, a GPU-accelerated workstation containing 20 physical Intel XeonCPU cores and two GeForce GTX 1080 TI graphics cards, totalling to 7200 CUDA cores. A system containing 256 POPC and 7 DMPS lipids evenly sectioned across each leaflet was prepared using the CHARMM-GUI builder. The system was equilibrated at a hydration of 25 water molecules per lipid molecule for 200 ns before the natural compounds were added into the water layer by a modified InflateGRO algorithm for multicomponent bilayers. Topologies for all systems were generated with the CHARMM General Force Field (CGenFF) program. All simulations were performed using the GROMACS 5.1.4 software package,[58,59] utilizing the CHARMM36 force field. All simulations used a 2 fs time step, periodic boundary conditions in all directions, a short-range van der Waals cutoff of 1.2 nm, the particle-mesh Ewald solution for long-range electrostatics,[60] and the LINCS algorithm for determination of bond constraints.[61] A Nose–Hoover thermostat at 30 °C (with a time constant of $\tau = 1$ ps) was used for temperature coupling,[62] while a Parrinello–Rahman semi-isotropic weak pressure coupling scheme was used to maintain a pressure of 1.0 bar (with a time constant of $\tau = 1$ ps).[63] The position of the molecules was restrained during volume (NVT) and pressure (NPT) equilibration to avoid free space bias as systems were reduced. Restraints were removed during 200 ns simulation. A total of 2 µs of simulations were run including 200 ns long, all-atom simulation runs for all compounds. Standard GROMACS scripts were used to extract the membrane width and the deuterium order parameter of the different membrane assays from the MD trajectories.

2.5. Microscopy

Fluorescent and optical microscopy were conducted using an Eclipse LV100 ND Microscope from Nikon in the Origins of Life Laboratory at McMaster University. The instrument was equipped with a Tu Plan Fluor BD 50× objective with a numerical aperture of 0.8. Images were recorded using a Nikon DS-Ri2 Camera with a resolution of 4908 × 3264 pixel and a pixel-size of 7.3 × 7.3 µm. The camera was mounted via a 2.5× telescope to the microscope. All images were recorded in episcopic illumination mode using a halogen lamp. Due to the high numerical aperture, the objective has a small depth of focus. This setup allows to measure 3D images to determine height profile and topology. In order to record a uniform sharp image, the Nikon control software (NIS Elements, Version 4.60.0) was used to record an extended depth of focus (EDF) image by combining multiple images with different focal planes. Bright field, dark field, and fluorescent images were taken for all samples. A B-2A long pass emission filter cube was used with an excitation wavelength of 450–490 nm and a long-pass analyzing filter with a barrier wavelength of 520 nm. Due to their auto-fluorescence, peptides light up in the fluorescent picture. Phospholipids, on the other hand, barely emit a fluorescent signal such that Aβ enriched regions can be identified on the fluorescent image. This technique has been used previously to study Aβ peptide-rich areas in POPC/DMPS bilayers.[53]

2.6. X-Ray Diffraction

X-ray diffraction data was obtained using the Biological Large Angle Diffraction Experiment (BLADE) at McMaster University. BLADE used a 9 kW (45 kV, 200 mA) CuKα rotating anode at a wavelength of 1.5418 Å using a Rigaku HyPix-3000 2D semiconductor detector with an area of 3000 mm^2 and 100 µm pixel size.[54] Diffraction measurements were conducted under controlled temperature and humidity conditions (30 °C, 98% RH) in a custom-built humidity chamber. The highly oriented membranes were aligned in the diffractometer such that the vertical axis (q_z) in the 2D scans was aligned perpendicular to the membranes and detected structure normal to the bilayers. Molecular structure in the plane of the membranes was detected along the horizontal axis ($q_{||}$). Using this setup, in-plane and out-of-plane structures can be determined separately but simultaneously. All samples were prepared and measured in replicates to check for consistency. The data presented in this work were the result of individual diffraction experiments conducted on individual membrane samples. Several samples were prepared for each compound and preparation protocols were refined until the experimental results between different samples of the same compound gave not more than 3% deviation. These results were taken to determine the total experimental errors.

The lamellar spacing, that is, the distance between membranes in the membrane stack (the thickness of the membrane plus water layer) was directly determined from the spacing of the lamellar Bragg peaks. The membrane thickness, defined as the distance between the head groups of the bilayers, was determined from the electron density, ρ_e along the bilayer normal, which was calculated through a Fourier transform of the integrated peak intensities.

To determine the degree of orientation of the membranes, the correlation peak intensities were integrated as a function of the meridional angle φ (the angle relative to the q_z axis, as sketched in Figure 5a). The corresponding intensity was fit with a Gaussian distribution centered at 0, which was then used to calculate the degree of orientation using Hermans orientation function

$$H = \frac{3 < \cos^2 \delta > -1}{2} \quad (1)$$

$H = 1.0$ corresponded to lipids which were perfectly parallel to each other within the bilayer (hyperordered), whereas $H = 0.25$ corresponded to a membrane with lipids in complete disorder.

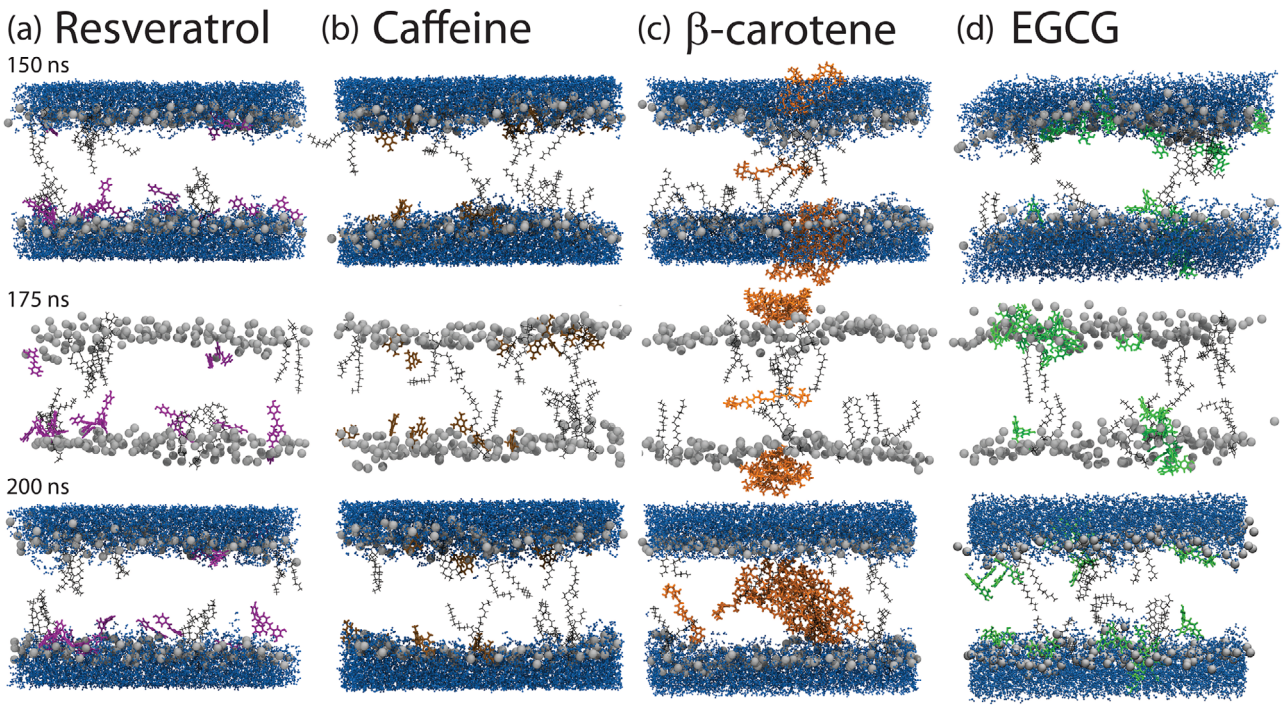

Figure 3. Snapshots of the MD simulations at different times for all compounds. a) Resveratrol and b) caffeine spontaneously partition in the membranes and position in the head group region of the bilayers. c) β-carotene and d) EGCG molecules were found to cluster in the water layer outside the membranes before entering the bilayers. While EGCG clusters were found in the head group region, β-carotene clusters eventually penetrate the membranes and partition in the hydrophobic membrane core.

2.7. UV–Visible Spectroscopy

UV–vis spectroscopy was conducted using a Nanophotometer (IMPLEN NP80). Liposome samples were used with the addition of trace amounts of ThT to each sample. The ThT assay is commonly used for the detection of amyloid fibrils.[64] The ThT class of molecules had several binding sites and bound to cross-strand ladders that were inherent in repeating side-chains interactions running across the β-strands within a β-sheet layer.[65–67] First, liposomes of POPC/DMPS (97:3 mol/mol%) were prepared and added 20 mol% Aβ_{25-35} and ThT to form peptide aggregates. Because ThT can accelerate deposition of Aβ peptides,[68] experiments without the presence of compounds were conducted over a period of 24 h to check for aggregation. Samples of Aβ_{25-35} were mixed in a 1.5 mL flask and kept in a shaking incubator at 37 °C. Aliquots were taken and placed in a cuvette at each time point. ThT was then added to the aliquot and a measurement was conducted. As ThT was found to induce aggregation, which plateaued out after 12 h,[54] all measurements were conducted 12 h after ThT deposition at 30 °C and all data were normalized to the ThT reference.

The corresponding spectrum shows absorption at 420 nm, characteristic of cross-β sheets. After a stable fluorescence was reached, appropriate volumes of resveratrol, caffeine, β-carotene, and EGCG were added to the solution. Water was used as a blank, and five 1.2 µl sample measurements were taken for each compound. Complete wave scans were measured and normalized for a wavelength range of 200–800 nm, and ThT absorption around a wavelength of 420 nm was monitored for each solution.

3. Results

3.1. Molecular Dynamics Simulation

Snapshots of the MD simulations are shown in **Figure 3** for (a) resveratrol, (b) caffeine, (c) β-carotene, and (d) EGCG at different times. Videos of the full simulations are provided as Supporting Information. All compounds were found to spontaneously partition into the membranes within the first 150 ns of the simulations. The smaller molecules, resveratrol and caffeine, were found to mainly position in the head–tail interface of the membranes while some were also temporarily found inside the hydrophobic core. The larger molecules, β-carotene and EGCG, were found to cluster in the water layer outside the membrane before making contact and partitioning. While EGCG molecules stay attached to the head group region, the β-carotene clusters eventually enter the membrane core (Figure 3c) and form stable transmembrane clusters. From the MD simulations one can conclude that all compounds are membrane active and spontaneously partition in the synthetic brain membranes. Membrane width (defined as the head group–head group distance) and the deuterium order parameter for all compounds were determined and are listed in **Table 1**. The deuterium order parameter is a measure of the mobility of the lipid acyl tails in the membrane core and was averaged for carbon atoms 7–16 in the POPC tails, in the center of the membrane core. While resveratrol and caffeine did not have a significant effect on the order parameter within the resolution of the simulations, β-carotene led to an increase of the lipid tail order, likely as a consequence of the transmembrane

Table 1. Structural membrane parameters for membranes containing different compounds with and without Aβ_{25-35}.

	Pure membrane			Membrane with Aβ_{25-35}	
	Membrane thickness [Å]	Membrane orientation [%]	Deuterium order parameter	Membrane thickness [Å]	Membrane orientation [%]
POPC/DMPS	37.2 ± 0.2#	74 ± 1.0#	0.149 ± 0.002*	37.6 ± 0.2#	74 ± 1.0#
	37.6 ± 0.2*				
+Resveratrol	41.2 ± 0.2#	96 ± 0.4#	0.144 ± 0.002*	38.8 ± 0.2#	80 ± 1.3#
	38.3 ± 0.2*				
+Caffeine	37.8 ± 0.2#	94 ± 0.7#	0.146 ± 0.002*	38.3 ± 0.2#	84 ± 0.7#
	38.3 ± 0.2*				
+β-Carotene	37.4 ± 0.2#	81 ± 1.2#	0.155 ± 0.002*	38.5 ± 0.2#	76 ± 0.5#
	38.8 ± 0.2*				
+EGCG	37.0 ± 0.2#	74 ± 1.8#	0.143 ± 0.002*	37.1 ± 0.2#	71 ± 1.2#
	38.3 ± 0.2*				

Parameters determined from MD simulations are marked with an asterisk (*) and results from X-ray diffraction with an (#). While MD simulations were conducted in the absence of Aβ, experimental parameters were obtained both with and without the peptide.

clusters, which constraint motion of the lipid tails. Lastly, EGCG led to an increase in lipid tail mobility.

3.2. Microscopy

Microscope images for all compounds are shown in **Figure 4**. All microscope images were recorded as 3D images that include information about sample height and topology. Figure 4a shows a bright field image of pure a POPC/DMPS sample, which exhibits a smooth and aggregate free surface. The membranes form homogeneous plateaus of about 50 µm in size. The corresponding height profile was determined from the 3D microscope images and a total surface height variation of ±4 µm was found (Figure S1a, Supporting Information). The addition of 20 mol% Aβ_{25-35} resulted in the formation of peptide-rich areas, which emit a strong fluorescence signal and are clearly visible on the fluorescent image. The addition of resveratrol in Figure 4b resulted in larger homogeneous membrane plateaus (about 100 µm in size), with larger height differences between neighboring plateaus. The height profile (Figure S1b, Supporting Information) shows a height difference of 25 µm between highest and lowest points. In the presence of Aβ_{25-35}, large peptide-rich clusters are observed in the fluorescent image. From the 3D image (Figure S2a, Supporting Information), these clusters are located on the surface of the membrane stack.

The addition of caffeine to the POPC/DMPS membranes in Figure 4c resulted in a smoother membrane surface, with a height variation of ±2 µm. The Aβ_{25-35} peptides were found to form pronounced amyloid fibrils, which are located on top of the membranes (Figure S2b, Supporting Information). Large β-carotene-rich membrane areas were observed in Figure 4d and Figure S1d, Supporting Information, which can easily be identified by their orange color. After the addition of Aβ_{25-35}, peptide-rich and β-carotene-rich areas become visible, which are evenly distributed. Lastly, large patches were observed in Figure 4e, that we tentatively assign to EGCG clusters. These areas embedded into the membranes by about 25 µm (Figure S1e, Supporting Information). When added to membranes containing Aβ_{25-35}, the fluorescent image shows smaller peptide-rich membrane areas. In contrast to the pure POPC/DMPS membranes, these areas appear more uniformly distributed.

3.3. X-Ray Diffraction

The result of the X-ray measurements are 2D diffraction maps for all compounds, that cover the signals of the membranes and the Aβ peptides, as shown in **Figure 5**a. Initial powder scattering of Aβ showed two diffuse bands in resultant reciprocal space corresponding to distances of 4.8 and 10 Å , respectively. Such signals agree with a pattern of β-strands running in-register to one another, as shown in Figure 5a. The X-ray diffraction pattern of cross-β sheets consists of two signals. The first peak, corresponding to a length scale of 10 Å represents the interactions that happen in between β-sheets, and are indicative of cross-β sheets. The length scale of 4.8 Å represents the interactions within a single β-sheet. The X-ray experiments, therefore, provide two signals: one from the presence of β-sheets and a second one when these β-sheets organize into cross-β sheets. The integrated intensity of the signals is a direct measure of the volume fraction of the corresponding structures. Additional signals (in the left bottom corner, at small $q_{||}$ and q_z values) occur in the 2D data related to the lamellar stacking of the bilayers. The packing of the acyl tails in the hydrophobic membrane core leads to an in-plane signal at about 4.6 Å ($q_{||} = 1.5$ Å^{-1}), as described in ref. [69].

Diffraction of the pure POPC/DMPS membranes is shown in Figure 5b. A series of well-developed Bragg peaks along q_z is the signature of well-organized lamellar membranes. The more diffuse circular intensity around the reflectivity Bragg peaks is the result of local membrane curvature. Membrane width and membrane orientation were determined from the out-of-plane scattering data (as detailed in the Experimental Section) and the corresponding values are listed in Table 1. A single lipid peak at $q_{||} \sim 1.5$ Å^{-1} is indicative of a homogeneous mixing of the two lipid components, without any phase separation. The addition of 20 mol% Aβ_{25-35} resulted in the formation of cross-β sheets and

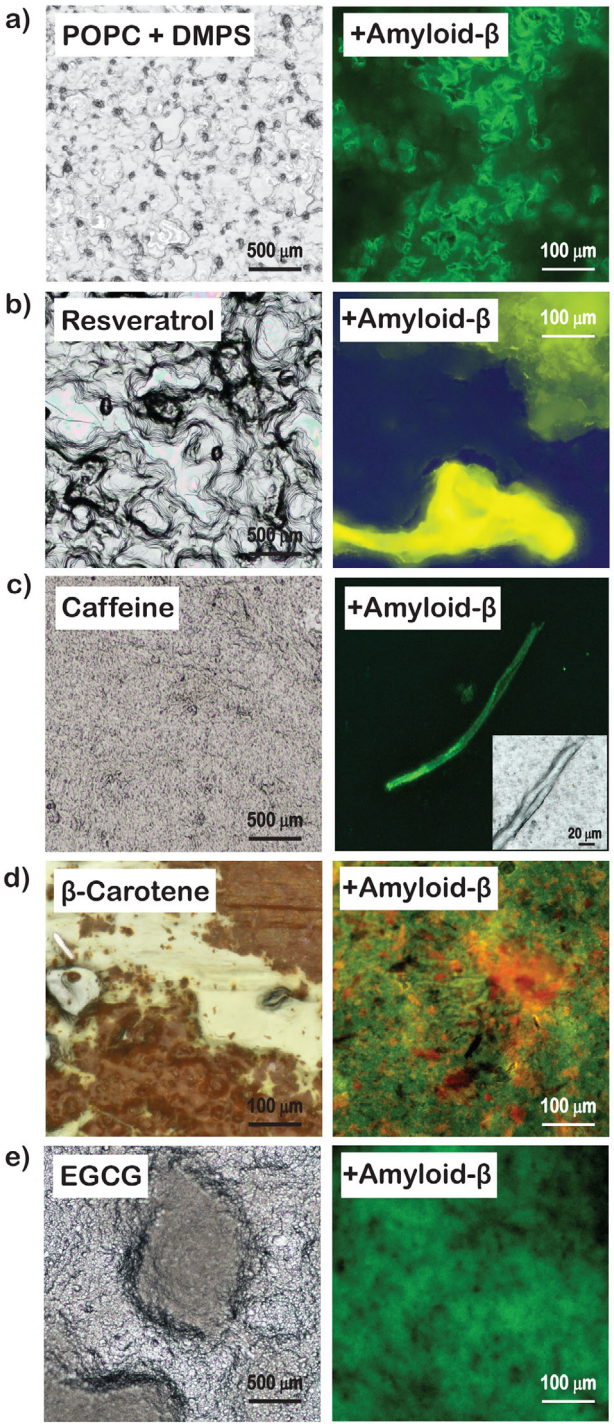

Figure 4. Microscope images of membranes with the addition of different compounds. a) POPC/DMPS formed a smooth and aggregate free surface. Addition of Aβ resulted in the formation of peptide-rich areas in the fluorescent image. b) Resveratrol resulted in larger membrane plateaus and large peptide-rich clusters, located on top of the membranes. c) Caffeine formed uniform and homogeneous membranes while well pronounced peptide fibrils were observed in the presence of Aβ. d) Large β-carotene-rich areas were found, and the addition of Aβ_{25-35}, resulted in peptide-rich and β-carotene-rich areas, which are evenly distributed. e) Large patches are observed with EGCG, which are likely to be enriched in such compounds. Peptide-rich, uniformly distributed membrane areas were found with the addition of Aβ.

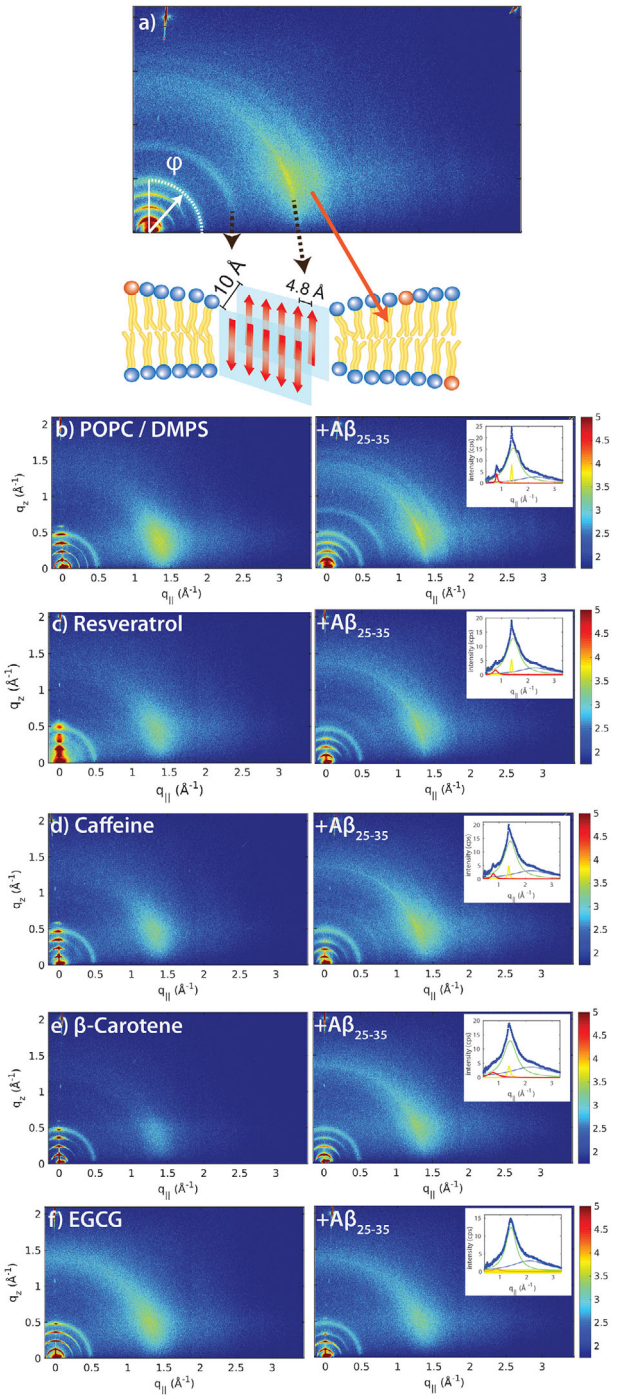

Figure 5. 2D X-ray diffraction for all compounds. a) In addition to signals from the membranes, two peptide signals are observed and assigned to the presence of cross-β sheets (at 10 Å) and β-sheets (at 4.8 Å). The Bragg peaks were radially integrated along the meridional angle φ to determine Hermans orientation function. b) Pure POPC/DMPS membranes show membrane signals related to the stacking of the bilayers in the membrane stack, and the packing of the acyl chains in the hydrophobic membrane core. Signals related to the formation of cross-β and β-sheets appear after the addition of 20 mol% Aβ_{25-35}. Well-organized membranes also form in the presence of c) resveratrol, d) caffeine, e) β-carotene, and f) EGCG, in agreement with the MD simulations. While cross-β and β-sheet signals are still visible after the addition of resveratrol and caffeine, there is a significant decrease in the cross-β signal with β-carotene and a significant decrease in cross-β and β-sheet signals with EGCG.

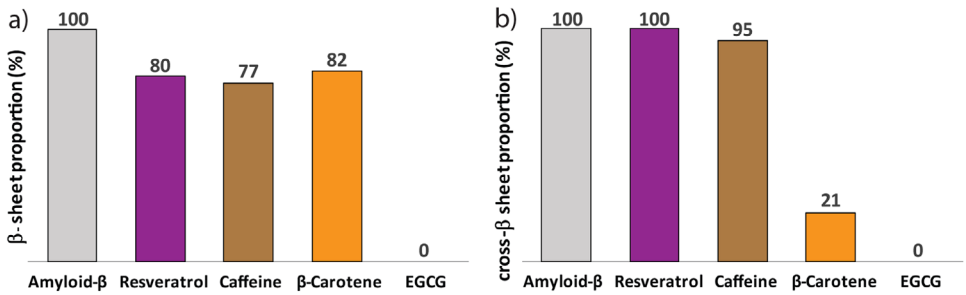

Figure 6. Integrated intensities of the a) β-sheet b) and cross-β sheet peptide signals as determined from the X-ray diffraction data in Figure 3. All compounds led to a slight decrease in β-sheets. A significant decrease in cross-β signal was observed for β-carotene, indicating that β-carotene is able to break up cross-β sheets, however, not β-sheets. No β-sheet or cross-β sheet signal was detected for EGCG indicating that EGCG completely dissolved the corresponding structures within the resolution of the experiment.

the corresponding signals appear in the diffraction pattern. The 2D data were integrated and converted into line scans, shown as insets. The yellow peak represents β-sheet interactions, and red peaks represent cross-β sheet interactions. The volume fraction of peptides in β and cross-β sheets are directly proportional to the corresponding integrated peak intensities. Values for all compounds are plotted in **Figure 6**.

Homogeneous membranes formed when resveratrol was added in Figure 5c, as indicated by the absence of additional signals or splitting of existing peaks, in agreement with the MD results. The broadening of the Bragg peaks is likely a sign of less well-organized membrane stacks, as also seen in the microscope images. Cross-β and β-sheets signals appeared when Aβ_{25-35} was added. Also the addition of β-carotene in Figure 5d did not disrupt the formation of membranes and a well-ordered lamellar membrane phase. However, a significant decrease in the cross-β signal is observed in the presence of Aβ. EGCG is also well absorbed by the brain membrane mimics in Figure 5e, in agreement with the computer simulations. The absence of cross-β and β-sheet signals with Aβ, however, points to a disaggregation of the peptide aggregates.

By comparing the integrated cross-β and β-sheet signals in Figure 6, all compounds resulted in a slight decrease in the amount of β-sheets present. In addition, β-carotene and EGCG resulted in a decrease of cross-β sheets with no cross-β sheet signal being detected for EGCG.

Values for membrane thickness and membrane orientation are listed in Table 1. While a membrane orientation of 100% is indicative of perfectly flat and stiff membranes, smaller values are the result of increased membrane fluidity and increased local curvature. In agreement with the MD simulations, resveratrol and caffeine induced thickening of the membranes and a significant decrease of membrane fluidity. β-carotene and EGCG, on the other hand, both slightly reduced membrane thickness and increased fluidity of the bilayers.

There was no difference in membrane thickness and fluidity in the presence of Aβ aggregates for the pure membrane. The addition of resveratrol and caffeine in led to a slight thickening of the membranes, and an increase of local membrane curvature, likely induced by the formation of extracellular amyloid aggregates and fibrils. The value for the membrane orientation with β-carotene of is significantly lower than the membrane orientation in the pure membranes likely indicating some bending to accommodate the peptide aggregates. The membranes containing peptides and EGCG were significantly thinner with increased local curvature, as compared to all other compounds.

3.4. UV–Visible Spectroscopy

The thioflavin T (ThT) fluorescence assay is frequently used for the detection of amyloid-β.[70] ThT is a β-sheet ligand which binds to amyloid fibrils such that their long axes are parallel, running along the length of the β-sheet.[71] The corresponding spectra for all compounds in **Figure 7** show a peak in absorbance around 420 nm, characteristic of β-sheets. While the addition of resveratrol in Figure 7a was found to lead to a slight increase in the fluorescent signal, a significant increase was observed after the addition of caffeine. This is likely the result of the formation of fibrillar structures, as seen in the microscope images, which increase ThT binding. Approximately no change was observed in the signal of β-carotene, and a decrease in β-sheet signal was observed with the addition of EGCG.

We note that the UV–vis measurements were conducted using liposomes made of POPC/DMPS containing 20 mol% Aβ_{25-35}. The different compounds were then added to the liposome solution. This liposome assay was prepared to confirm the findings in a more cellular context. Differences in the observations and measured parameters between the results from the X-ray diffraction will be discussed in detail below.

4. Discussion

Natural compounds including resveratrol, caffeine, β-carotene, and EGCG have been reported to inhibit Aβ formation and aggregation, but the exact mechanisms are often unclear. Some compounds have been shown to interact with Aβ peptides directly, but it is uncertain whether this is due to the experimental setup or due to natural interactions. For instance, Wang et al.[28] reported that both resveratrol and EGCG interact directly with Aβ either via a sequence specific interaction, in the case of EGCG, or via a hydrophobic side-chain association, in the case of resveratrol. Similarly, Sharma and Paul[36] reported a similar interaction between Aβ and caffeine, where caffeine interacts with the aromatic residues found in the peptide, thus restricting its interaction with other peptides. These results were obtained from MD

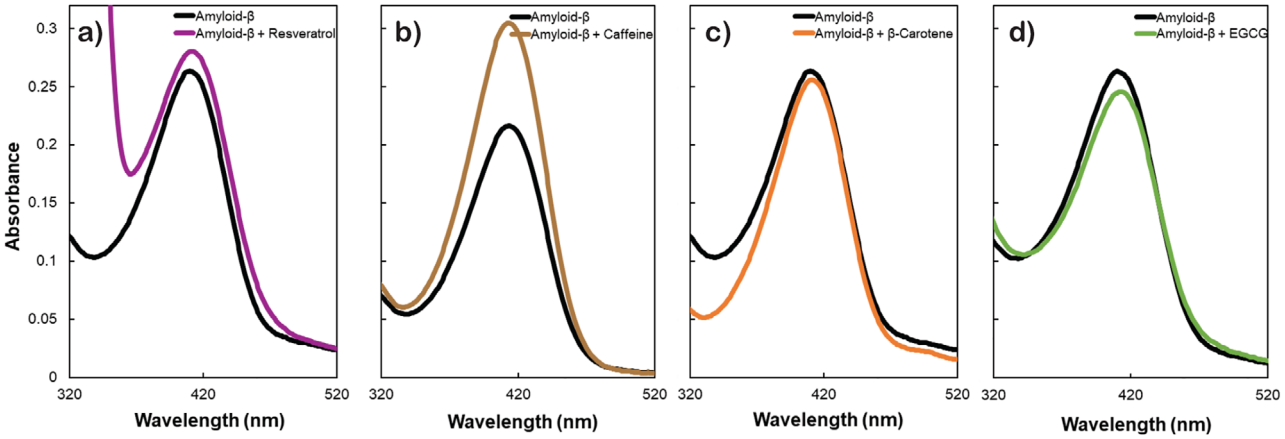

Figure 7. ThT absorbance spectra for membranes containing $A\beta_{25-35}$ in the presence of a) resveratrol, b) caffeine, c) β-carotene, and d) EGCG. Spectra of pure POPS/DMPS + 20 mol% $A\beta_{25-35}$ are plotted as reference in black. Resveratrol and caffeine led to an increase in the ThT signal, which is indicative of an increase in β-sheet and cross-β sheet structures. Lastly, while no change was observed for β-carotene, the β-sheet signals were found to decrease after the addition of EGCG.

simulations which only contained the peptide and the compound and may, therefore, overestimate the corresponding interactions. This is similar to the case of Aβ and β-carotene, where aggregation experiments were conducted using only the peptide and the compound, perhaps overestimating a potential interaction.[40]

In this study, we explored a different pathway for interaction and investigated a potential membrane-mediated interplay. Such an interaction can occur when both the compound and the peptide aggregates partition in membranes at the same time. This is, in particular, the case for the early stages of Aβ plaque formation, which have been reported to occur through membrane interactions.[22,72] These include elastic interactions, such as membrane bending and distortions, as well as changes in membrane fluidity, which can all significantly change aggregation forces.[53,69,72,73]

This work uses synthetic membrane mimics to investigate a membrane-mediated interaction between resveratrol, caffeine, β-carotene, and EGCG with $A\beta_{25-35}$ aggregates, which form through their interaction with lipid membranes. The $A\beta_{25-35}$ fragment is primarily hydrophobic and embeds itself into the hydrophobic core of the membrane and is considered the membrane-active segment, often used in membrane studies. Such simplistic systems are typically used in a biophysical approach. A reduction in the number of parameters and variables goes along with a high, molecular resolution. While using human tissue and the full-length peptides $A\beta_{1-40}$ and $A\beta_{1-42}$ for these experiments is certainly of greater physiological relevance, it is very difficult to conduct simulations and experiments in these systems and uniquely assign signals to the different molecular components and processes. Also, while the different food types contain more compounds than just the molecules that we investigated, a simplistic approach gives a higher level of molecular information.

We note that while the MD simulations provided a very detailed picture of the interaction between the compounds and the membranes, MD simulations were not conducted to study the interaction between the compounds and Aβ aggregates. Modeling peptide aggregation in computer simulations, and the corresponding changes in secondary peptide structure, is a challenging task even on today's supercomputers, which require large systems, long simulation times, and in particular, the exact knowledge of the underlying force fields.[74–76]

From the MD simulations, all compounds were found to be membrane active and to mainly partition in the head group region of the membranes, with the exception of β-carotene which formed transmembrane domains. While some compounds, such as resveratrol and caffeine, led to membrane thickening and reduced fluidity, β-carotene and EGCG both made the membranes more fluid and thinner. This was confirmed by microscopy and X-ray data. It is important to note that none of the compounds were found to disrupt the bilayers or led to pore formation at the concentrations used. In summary, while resveratrol and caffeine dissolved in the membranes and made them thicker and less fluid, β-carotene and EGCG were found to have a tendency to aggregate and form separate, enriched membrane domains, making the membranes thinner and more fluid.

When comparing these findings with the current literature it becomes evident that no conclusive statements can be proposed. Caffeine for instance was previously reported to reduce membrane fluidity, increase membrane thickness, and attract water molecules.[77] Resveratrol has been found to permeate the membrane both in the acyl region and in the head group region of the membrane, as well as to have a membrane fluidizing effect.[78] Similarly, Neves et al.[79] found that resveratrol may either make the membrane fluid or stiff, depending on its fluidity state, thus resembling cholesterol. Previous studies have reported that β-carotene inserts itself into the membrane, having its polar groups anchored in the opposite polar zones of the membrane and that it rigidifies the fluid phase of the membrane.[80] Conversely, it has been found to be oriented deep inside the hydrophobic membrane, parallel to the membrane surface.[81] Lastly, β-carotene has also been found to form aggregates in the membrane.[82] The literature on EGCG's interaction with the lipid bilayer is somewhat scarce. Sun et al.[83] have reported that it readily binds to the membrane and that it solubilizes lipid molecules without forming pores, while Tamba et al.[84] have reported that it leads

to the gradual leakage of internal contents. However, even though these compounds have been reported to have various different effects on the membrane, it is still important to note that they may also exhibit physiological effects that have not been taken into account in this study. For instance, it is known that polyphenols, such as resveratrol and EGCG, respond in a dose-dependent manner, a process termed hormesis (for a review see refs. [85, 86]). Thus, investigating the effects of these compounds at different concentrations may be of extreme importance.

The different compounds were found to have distinct effects on Aβ plaques. A summary of the interpretation of the experimental findings is shown in **Figure 8**. Micrometer-sized cross-β sheets were observed at elevated concentrations of Aβ. Peptide-rich areas appeared on the fluorescent microscope images and β-sheet and cross-β signals were visible in the X-ray experiments. This cross-β sheet structure is in agreement with the structure of amyloid fibrils reported in the literature[18,19] and small, nanometer-sized membrane embedded β-sheets have been proposed to serve as nuclei for extracellular fibril growth.[17] In summary, the presence of lipid membranes seems crucial in triggering or accelerating amyloid aggregation.[22,87–90]

Peptide-rich clusters were found to form on top of the membranes in the presence of resveratrol, consisting of β-sheets and cross-β sheets. Caffeine was found to expel the peptides from the membranes, leading to the formation of pronounced amyloid fibrils, which can be clearly seen on the microscope images and by their distinct β-sheet and cross-β signals. As the X-ray measurements provide two separate signals on the length scale of cross-β sheets (the 10 Å signal) and β-sheets (signal at 4.8 Å), the impact of the different molecules can be studied for both structures separately but simultaneously. Lastly, both β-carotene and EGCG were found to reduce the size and volume fraction of the Aβ aggregates.

The UV–vis experiments using liposomes in solution corroborate and validate these findings in a cellular context. The addition of resveratrol and caffeine to the liposomes containing Aβ plaques led to an increase in the ThT absorbance related to an enhancement of the β-sheet structure. Conversely, a decrease in the 420 nm signal was observed when EGCG was added to the liposome solution, and almost no change was observed with the addition of β-carotene. While these observations are in agreement with the findings in the membrane stacks, the β-sheet signals show much smaller decreases. This is likely due to the fact that the membrane assay may overestimate the partitioning of the different compounds. When the stacks are prepared, the molecules are trapped in a relatively thin, about 2 nm thick, water layer between the stacked membranes and interact with them on a short timescale. When the molecules are added to the liposome solution, however, the equilibrium between molecules adsorbed to, or absorbed into the bilayers with respect to molecules in solution is likely shifted toward the dissolved molecules. This may result in a smaller partitioning coefficient, leading to a smaller effect, as observed.

The experimental and computational observations led us to the following conclusion: Thickening and stiffening of the membrane resulted in the expulsion of the peptide aggregates, as observed for resveratrol and caffeine. Thinning and fluidification of the membranes dissolved the β- and cross-β sheets in the presence of EGCG. β-carotene presents a somewhat intermediate case as it did increase fluidity, however, also formed transmembrane aggregates inside the membranes, which resulted in breaking up cross-β sheets into small β-sheets. At this point, the full mechanism for membrane-mediated Aβ aggregation remains elusive. However, from our current understanding, membranes provide a crucial framework for the processes involved in aggregation. At the early stages of peptide aggregation, the bilayer offers a site of high stability for the Aβ monomers, which allows neighboring peptides to coordinate hydrogen-bonding and folding and uncoiling of the peptide to form more stable β- and

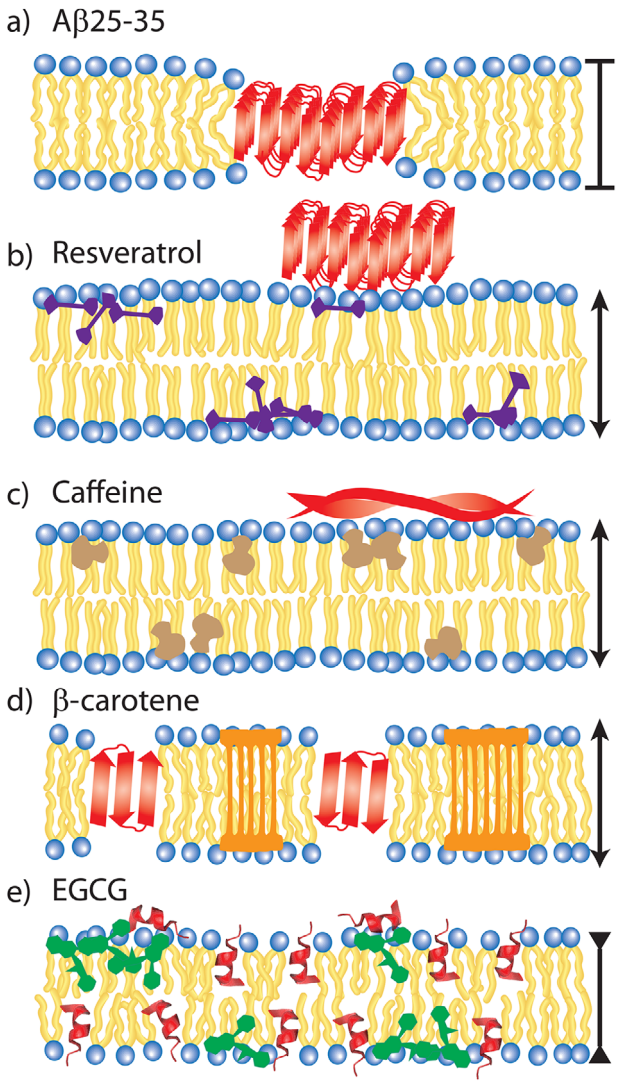

Figure 8. Summary and interpretation of findings. The different compounds change membrane thickness and membrane fluidity, which impact Aβ aggregation in different ways. Values for membrane width and orientation were determined from X-ray diffraction. a) Aβ_{25-35} displays the classic aggregation model. b) Resveratrol and c) caffeine make membranes thicker, less fluid, and expel the Aβ peptides from the membrane leading to the formation of plaques and fibrils located on top of the membranes. d) β-carotene partially preserves membrane fluidity and smaller Aβ domains made of β-sheets are observed. Lastly, e) EGCG preserves membrane thickness and fluidity and was found to dissolve β- and cross-β sheets.

cross-β sheets. These processes make the membrane a key component in the nucleation of peptide aggregates.

Membrane properties, such as thickness, fluidity, spontaneous curvature, and elastic constants, reduce the Gibbs energy for aggregation by providing the Aβ peptide an environment which reduces the entropy of the aggregated peptide. An increase in membrane fluidity can in particular reduce the hydrophobic mismatch that occurs when the hydrophobic region of the peptides is larger or smaller than the bilayers' hydrophobic thickness, which causes each monolayer leaflet to distort in order to ensure the entire hydrophobic region of the peptide is contained within the hydrophobic core. The findings in this work further support this model. Amyloid plaques are still a prime target for pharmaceutical development as existing pharmaceutical approaches are still mostly focused on the design and synthesis of therapeutics to inhibit pathological oligomerization of Aβ and tau proteins. This approach should likely include drug candidates that target the membrane environment to explore if they can inhibit and potentially even reverse the formation of amyloid clusters.

5. Conclusions

Micrometer-sized peptide aggregates consisting of cross-β sheets of $A\beta_{25-35}$ were created in synthetic brain membranes, which resemble the plaques of Alzheimer's patients. We studied the impact of resveratrol, caffeine, β-carotene, and EGCG, on these amyloid aggregates using optical and fluorescence microscopy, X-ray diffraction, UV–vis spectroscopy, and molecular dynamics (MD) simulations. All compounds were found to be membrane active and spontaneously partitioned in the synthetic brain membranes. While resveratrol and caffeine led to membrane thickening and reduced membrane fluidity, β-carotene and EGCG preserved or increased fluidity, respectively. In the presence of Aβ plaques, resveratrol and caffeine did not reduce the volume fraction of cross-β sheets but led to their expulsion from the membranes. β-carotene significantly reduced plaque size and volume fraction of cross-β sheets by 80%, while keeping the number of β-sheets constant. Lastly, EGCG significantly decreased cross-β and β-sheet signals, indicative of the dissolution of peptide aggregates.

It has become clear that membranes may play a crucial role in the early stages of peptide aggregation in Alzheimer's disease. While the compounds used in this study were all ingredients of natural products, synthetic molecules will also be designed and tested in the future to develop a new, indirect, membrane-mediated pathway for the development of anti-Alzheimer's drugs.

Supporting Information

Supporting Information is available from the Wiley Online Library or from the author.

Acknowledgements

This research was funded by the Natural Sciences and Engineering Research Council of Canada (NSERC), the National Research Council Canada (NRC), the Canada Foundation for Innovation (CFI), and the Ontario Ministry of Economic Development and Innovation. M.C.R. is the recipient of an Early Researcher Award of the Province of Ontario and a University Scholar of McMaster University. The funders had no role in study design, data collection and analysis, decision to publish, or preparation of the manuscript.

Data Availability Statement

The data that support the findings of this study are available from the corresponding author upon reasonable request.

Conflict of Interest

The authors declare no conflict of interest.

Keywords

Alzheimer's disease, amyloid-β peptides, β-carotene, caffeine, cross-β sheets, epigallocatechin gallate, nutrition, resveratrol

Received: July 2, 2020
Published online:

[1] C. P. Ferri, M. Prince, C. Brayne, H. Brodaty, L. Fratiglioni, M. Ganguli, K. Hall, K. Hasegawa, H. Hendrie, Y. Huang, A. Jorm, C. Mathers, P. R. Menezes, E. Rimmer, M. Scazufca, *Lancet* **2005**, *366*, 2112.
[2] C. L. Masters, G. Multhaup, G. Simms, J. Pottgiesser, R. Martins, K. Beyreuther, *EMBO J.* **1985**, *4*, 2757.
[3] I. Benilova, E. Karran, B. De Strooper, *Nat. Neurosci.* **2012**, *15*, 349.
[4] T. A. Pascoal, S. Mathotaarachchi, M. S. Kang, S. Mohaddes, M. Shin, A. Y. Park, M. J. Parent, A. L. Benedet, M. Chamoun, J. Therriault, H. Hwang, C. Cuello, B. Misic, J. P. Soucy, J. A. Aston, S. Gauthier, P. RosaNeto, *Nat. Commun.* **2019**, *10*, 2353.
[5] J. A. Hardy, G. A. Higgins, *Science* **1992**, *256*, 184.
[6] F. Kametani, M. Hasegawa, *Front. Neurosci.* **2018**, *12*, 25.
[7] F. Chiti, C. M. Dobson, *Annu. Rev. Biochem.* **2017**, *86*, 27.
[8] J. M. Long, D. M. Holtzman, *Cell* **2019**, *179*, 312.
[9] C. Haass, M. G. Schlossmacher, A. Y. Hung, C. Vigo-Pelfrey, A. Mellon, B. L. Ostaszewski, I. Lieberburg, E. H. Koo, D. Schenk, D. B. Teplow, D. J. Selkoe, *Nature* **1992**, *359*, 322.
[10] J. Kang, H. G. Lemaire, A. Unterbeck, J. M. Salbaum, C. L. Masters, K. H. Grzeschik, G. Multhaup, K. Beyreuther, B. Müller-Hill, *Nature* **1987**, *325*, 733.
[11] C. Haass, D. J. Selkoe, *Nat. Rev. Mol. Cell Biol.* **2007**, *8*, 101.
[12] R. J. O'Brien, P. C. Wong, *Annu. Rev. Neurosci.* **2011**, *34*, 185.
[13] G. Bitan, M. D. Kirkitadze, A. Lomakin, S. S. Vollers, G. B. Benedek, D. B. Teplow, *Proc. Natl. Acad. Sci. U. S. A.* **2003**, *100*, 330.
[14] R. P. Mason, J. D. Estermyer, J. F. Kelly, P. E. Mason, *Biochem. Biophys. Res. Commun.* **1996**, *222*, 78.
[15] S. Dante, T. Hauss, N. A. Dencher, *Biophys. J.* **2002**, *83*, 2610.
[16] S. Dante, T. Hauß, N. A. Dencher, *Eur. Biophys. J.* **2006**, *35*, 523.
[17] D. Eisenberg, M. Jucker, *Cell* **2012**, *148*, 1188.
[18] A. W. Fitzpatrick, G. T. Debelouchina, M. J. Bayro, D. K. Clare, M. A. Caporini, V. S. Bajaj, C. P. Jaroniec, L. Wang, V. Ladizhansky, S. A. Müller, C. E. Macphee, C. A. Waudby, H. R. Mott, A. De Simone, T. P. J. Knowles, H. R. Saibil, M. Vendruscolo, E. V. Orlova, R. G. Griffin, C. M. Dobson, *Proc. Natl. Acad. Sci. U. S. A.* **2013**, *110*, 5468.
[19] R. Nelson, M. R. Sawaya, M. Balbirnie, A. Ø. Madsen, C. Riekel, R. Grothe, D. Eisenberg, *Nature* **2005**, *435*, 773.

[20] S. I. Cohen, S. Linse, L. M. Luheshi, E. Hellstrand, D. A. White, L. Rajah, D. E. Otzen, M. Vendruscolo, C. M. Dobson, T. P. Knowles, *Proc. Natl. Acad. Sci. U. S. A.* **2013**, *110*, 9758.
[21] A. Cuco, A. P. Serro, J. P. Farinha, B. Saramago, A. G. da Silva, *Colloids Surf., B* **2016**, *141*, 10.
[22] A. Khondker, R. J. Alsop, M. C. Rheinstädter, *Membranes* **2017**, *7*, 49.
[23] W. K. Subczynski, A. Wisniewska, *Acta Biochim. Pol.* **2000**, *47*, 613.
[24] P. V. Escribá, J. M. González-Ros, F. M. Goñi, P. K. Kinnunen, L. Vigh, L. Sánchez-Magraner, A. M. Fernández, X. Busquets, I. Horváth, G. Barceló-Coblijn, *J. Cell. Mol. Med.* **2008**, *12*, 829.
[25] V. Martín, N. Fabelo, G. Santpere, B. Puig, R. Marín, I. Ferrer, M. Díaz, *J. Alzheimer's Dis.* **2010**, *19*, 489.
[26] S. S. Antollini, C. Fabiani, *Front. Cell. Neurosci.* **2019**, *13*, 309.
[27] P. Velander, L. Wu, F. Henderson, S. Zhang, D. R. Bevan, B. Xu, *Biochem. Pharmacol.* **2017**, *139*, 40.
[28] Y. Wang, D. C. Latshaw, C. K. Hall, *J. Mol. Biol.* **2017**, *429*, 3893.
[29] S. S. Karuppagounder, J. T. Pinto, H. Xu, H. L. Chen, M. F. Beal, G. E. Gibson, *Neurochem. Int.* **2009**, *54*, 111.
[30] P. Marambaud, H. Zhao, P. Davies, *J. Biol. Chem.* **2005**, *280*, 37377.
[31] Y. Feng, X. P. Wang, S. G. Yang, Y. J. Wang, X. Zhang, X. T. Du, X. X. Sun, M. Zhao, L. Huang, R. T. Liu, *Neurotoxicology* **2009**, *30*, 986.
[32] Y. Chen, G. W. Shi, Z. M. Liang, S. Y. Sheng, Y. S. Shi, L. Peng, Y. P. Wang, F. Wang, X. M. Zhang, *Mol. Med. Rep.* **2019**, *19*, 3783.
[33] L. Maia, A. De Mendonça, *Eur. J. Neurol.* **2002**, *9*, 377.
[34] G. W. Arendash, T. Mori, C. Cao, M. Mamcarz, M. Runfeldt, A. Dickson, K. Rezai-Zadeh, J. Tan, B. A. Citron, X. Lin, V. Echeverria, H. Potter, *J. Alzheimer's Dis.* **2009**, *17*, 661.
[35] G. Arendash, W. Schleif, K. Rezai-Zadeh, E. Jackson, L. Zacharia, J. Cracchiolo, D. Shippy, J. Tan, *Neuroscience* **2006**, *142*, 941.
[36] B. Sharma, S. Paul, *J. Phys. Chem. B* **2016**, *120*, 9019.
[37] O. P. Dall'Igna, P. Fett, M. W. Gomes, D. O. Souza, R. A. Cunha, D. R. Lara, *Exp. Neurol.* **2007**, *203*, 241.
[38] W. Wang, L. Shinto, W. E. Connor, J. F. Quinn, *J. Alzheimer's Dis.* **2008**, *13*, 31.
[39] F. J. Li, L. Shen, H. F. Ji, *J. Alzheimer's Dis.* **2012**, *31*, 253.
[40] J. Takasaki, K. Ono, Y. Yoshiike, M. Hirohata, T. Ikeda, A. Morinaga, A. Takashima, M. Yamada, *J. Alzheimer's Dis.* **2011**, *27*, 271.
[41] Y. Li, S. Liu, Y. Man, N. Li, Y. Zhou, *Exp. Ther. Med.* **2015**, *9*, 1489.
[42] D. E. Ehrnhoefer, J. Bieschke, A. Boeddrich, M. Herbst, L. Masino, R. Lurz, S. Engemann, A. Pastore, E. E. Wanker, *Nat. Struct. Mol. Biol.* **2008**, *15*, 558.
[43] J. Bieschke, J. Russ, R. P. Friedrich, D. E. Ehrnhoefer, H. Wobst, K. Neugebauer, E. E. Wanker, *Proc. Natl. Acad. Sci. U. S. A.* **2010**, *107*, 7710.
[44] Y. T. Choi, C. H. Jung, S. R. Lee, J. H. Bae, W. K. Baek, M. H. Suh, J. Park, C. W. Park, S. I. Suh, *Life Sci.* **2001**, *70*, 603.
[45] K. Rezai-Zadeh, D. Shytle, N. Sun, T. Mori, H. Hou, D. Jeanniton, J. Ehrhart, K. Townsend, J. Zeng, D. Morgan, J. Hardy, T. Town, J. Tan, *J. Neurosci.* **2005**, *25*, 8807.
[46] A. V. Witte, L. Kerti, D. S. Margulies, A. Flöel, *J. Neurosci.* **2014**, *34*, 7862.
[47] Y. N. Zhao, W. F. Li, F. Li, Z. Zhang, Y. D. Dai, A. L. Xu, C. Qi, J. M. Gao, J. Gao, *Biochem. Biophys. Res. Commun.* **2013**, *435*, 597.
[48] S. Hira, U. Saleem, F. Anwar, M. F. Sohail, Z. Raza, B. Ahmad, *Biomolecules* **2019**, *9*, 441.
[49] F. Grodstein, J. H. Kang, R. J. Glynn, N. R. Cook, J. M. Gaziano, *Arch. Intern. Med.* **2007**, *167*, 2184.
[50] K. Rezai-Zadeh, G. W. Arendash, H. Hou, F. Fernandez, M. Jensen, M. Runfeldt, R. D. Shytle, J. Tan, *Brain Res.* **2008**, *1214*, 177.
[51] M. Costa, P. Botton, S. Mioranzza, D. Souza, L. Porciuncula, *Neuroscience* **2008**, *153*, 1071.
[52] T. Zhang, J. Zhang, P. Derreumaux, Y. Mu, *J. Phys. Chem. B* **2013**, *117*, 3993.
[53] J. Tang, R. J. Alsop, M. Backholm, H. Dies, A. C. Shi, M. C. Rheinstädter, *Soft Matter* **2016**, *12*, 3165.
[54] A. Khondker, R. J. Alsop, S. Himbert, J. Tang, A. C. Shi, A. P. Hitchcock, M. C. Rheinstädter, *Sci. Rep.* **2018**, *8*, 12367.
[55] S. C. Jao, K. Ma, J. Talafous, R. Orlando, M. G. Zagorski, *Amyloid* **1997**, *4*, 240.
[56] H. Dies, L. Toppozini, M. C. Rheinstädter, *PLOS One* **2014**, *9*, e99124.
[57] M. A. Barrett, R. J. Alsop, T. Hauß, M. C. Rheinstädter, *Membranes* **2015**, *5*, 824.
[58] M. J. Abraham, T. Murtola, R. Schulz, S. Páll, J. C. Smith, B. Hess, E. Lindahl, *SoftwareX* **2015**, *1*, 19.
[59] D. Van Der Spoel, E. Lindahl, B. Hess, G. Groenhof, A. E. Mark, H. J. Berendsen, *J. Comput. Chem.* **2005**, *26*, 1701.
[60] T. Darden, D. York, L. Pedersen, *J. Chem. Phys.* **1993**, *98*, 10089.
[61] B. Hess, H. Bekker, H. J. Berendsen, J. G. Fraaije, *J. Comput. Chem.* **1997**, *18*, 1463.
[62] D. J. Evans, B. L. Holian, *J. Chem. Phys.* **1985**, *83*, 4069.
[63] M. Parrinello, A. Rahman, *J. Appl. Phys.* **1981**, *52*, 7182.
[64] S. A. Hudson, H. Ecroyd, T. W. Kee, J. A. Carver, *FEBS J.* **2009**, *276*, 5960.
[65] M. Biancalana, S. Koide, *Biochim. Biophys. Acta, Proteins Proteomics* **2010**, *1804*, 1405.
[66] I. M. Kuznetsova, A. I. Sulatskaya, V. N. Uversky, K. K. Turoverov, *PLOS One* **2012**, *7*, e30724.
[67] A. Lockhart, L. Ye, D. B. Judd, A. T. Merritt, P. N. Lowe, J. L. Morgenstern, G. Hong, A. D. Gee, J. Brown, *J. Biol. Chem.* **2005**, *280*, 7677.
[68] M. D'Amico, M. G. Di Carlo, M. Groenning, V. Militello, V. Vetri, M. Leone, *J. Phys. Chem. Lett.* **2012**, *3*, 1596.
[69] C. L. Armstrong, D. Marquardt, H. Dies, N. Kučerka, Z. Yamani, T. A. Harroun, J. Katsaras, A. C. Shi, M. C. Rheinstädter, *PLOS One* **2013**, *8*, e66162.
[70] H. Levine, III, *Protein Sci.* **1993**, *2*, 404.
[71] M. R. Krebs, E. H. Bromley, A. M. Donald, *J. Struct. Biol.* **2005**, *149*, 30.
[72] M. C. Rheinstädter, K. Schmalzl, K. Wood, D. Strauch, *Phys. Rev. Lett.* **2009**, *103*, 128104.
[73] C. L. Armstrong, E. Sandqvist, M. C. Rheinstadter, *Protein Pept. Lett.* **2011**, *18*, 344.
[74] C. Lockhart, A. K. Smith, D. K. Klimov, *J. Chem. Inf. Model.* **2020**, *60*, 2282.
[75] D. L. Parton, J. W. Klingelhoefer, M. S. Sansom, *Biophys. J.* **2011**, *101*, 691.
[76] V. Corradi, E. Mendez-Villuendas, H. I. Ingólfsson, R. X. Gu, I. Siuda, M. N. Melo, A. Moussatova, L. J. DeGagné, B. I. Sejdiu, G. Singh, T. A. Wassenaar, K. D. Magnero, S. J. Marrink, D. P. Tieleman, *ACS Cent. Sci.* **2018**, *4*, 709.
[77] A. Khondker, A. Dhaliwal, R. J. Alsop, J. Tang, M. Backholm, A. C. Shi, M. C. Rheinstädter, *Phys. Chem. Chem. Phys.* **2017**, *19*, 7101.
[78] J. Brittes, M. Lucio, C. Nunes, J. Lima, Y. Reis, *Chem. Phys. Lipids* **2010**, *163*, 747.
[79] A. R. Neves, C. Nunes, H. Amenitsch, S. Reis, *Soft Matter* **2016**, *12*, 2118.
[80] W. I. Gruszecki, K. Strzałka, *Biochim. Biophys. Acta, Mol. Basis Dis.* **2005**, *1740*, 108.
[81] M. Van de Ven, M. Kattenberg, G. Van Ginkel, Y. Levine, *Biophys. J.* **1984**, *45*, 1203.
[82] A. Shibata, Y. Kiba, N. Akati, K. Fukuzawa, H. Terada, *Chem. Phys. Lipids* **2001**, *113*, 11.
[83] Y. Sun, W. C. Hung, F. Y. Chen, C. C. Lee, H. W. Huang, *Biophys. J.* **2009**, *96*, 1026.
[84] Y. Tamba, S. Ohba, M. Kubota, H. Yoshioka, H. Yoshioka, M. Yamazaki, *Biophys. J.* **2007**, *92*, 3178.

[85] M. Leri, M. Scuto, M. L. Ontario, V. Calabrese, E. J. Calabrese, M. Bucciantini, M. Stefani, *Int. J. Mol. Sci.* **2020**, *21*, 1250.
[86] S. Miquel, C. Champ, J. Day, E. Aarts, B. A. Bahr, M. Bakker, D. Bánáti, V. Calabrese, T. Cederholm, J. Cryan, L. Dye, J. A. Farrimond, A. Korosi, S. Laye, S. Maudsley, D. Milenkovic, M. H. Mohajeri, J. Sijben, A. Solomon, J. P. E. Spencer, S. Thuret, W. Vanden Berghe, D. Vauzour, B. Vellas, K. Wesnes, P. Willatts, R. Wittenberg, L. Geurts, *Ageing Res. Rev.* **2018**, *42*, 40.
[87] C. Galvagnion, A. K. Buell, G. Meisl, T. C. Michaels, M. Vendruscolo, T. P. Knowles, C. M. Dobson, *Nat. Chem. Biol.* **2015**, *11*, 229.
[88] E. Drolle, A. Negoda, K. Hammond, E. Pavlov, Z. Leonenko, *PLOS One* **2017**, *12*, e0182194.
[89] D. J. Lindberg, E. Wesén, J. Björkeroth, S. Rocha, E. K. Esbjörner, *Biochim. Biophys. Acta, Biomembr.* **2017**, *1859*, 1921.
[90] M. Törnquist, T. C. Michaels, K. Sanagavarapu, X. Yang, G. Meisl, S. I. Cohen, T. P. Knowles, S. Linse, *Chem. Commun.* **2018**, *54*, 8667.